A Terrestrial Gamma-ray Flash from the 2022 Hunga Tonga–Hunga Ha'apai Volcanic Eruption

M. S. Briggs[1,2], S. Lesage[2], C. Schultz[3], B. Mailyan[4], R. H. Holzworth[5]

[1]Center for Space Plasma and Aeronomic Research (CSPAR), University of Alabama in Huntsville

[2]Dept. of Space Sciences, University of Alabama in Huntsville

[3]Earth Science Office, NASA Marshall Space Flight Center

[4]Center for Astro, Particle and Planetary Physics, New York University Abu Dhabi

[5]Earth and Space Sciences, University of Washington, Seattle, WA

Key Points:

- A TGF was detected from volcanic lightning from Hunga Tonga–Hunga Ha'apai, extending the types of storms that can produce TGFs.
- The observation of a single TGF is consistent with the volcanic lightning producing TGFs at the same rate as thunderstorm lightning.
- The observation of the TGF from space indicates that electrons were accelerated upward by the electric field within the volcanic plume.

Corresponding author: Michael S. Briggs, `Michael.Briggs@uah.edu`

Abstract

The Hunga Tonga–Hunga Ha'apai submarine volcano recently resumed activity. Violent eruptions on 2022 January 14th and 15th launched a tall ash plume that produced extremely high lightning rates. Here we report a terrestrial gamma-ray flash (TGF) that was produced by the volcanic lightning and observed from space by the Fermi Gamma-ray Burst Monitor (GBM). Observations by radio lightning networks and especially by the Geostationary Lightning Mapper (GLM) show that the only lightning close enough to produce a TGF detectable by Fermi GBM was from the volcano's plume. With the observing duration of Fermi, observing a single TGF is consistent with the hypothesis that the volcanic lightning of this eruption produced TGFs at the average rate of thunderstorm lightning. The observation of a strong TGF from space also indicates that the electric field was oriented so as to accelerate electrons upward.

Plain Language Summary

Terrestrial Gamma-ray Flashes (TGFs) are short, intense flashes of gamma-ray that are associated with lightning. Until now these flashes have only been associated with thunderstorms. High electric fields in thunderstorms accelerate electrons, which then produce gamma-rays that are observed by space-based detectors. On 2022 January 14th and 15th violent eruptions of the Hunga Tonga–Hunga Ha'apai volcano produced extremely high lightning rates. NASA's Fermi Gamma-ray Burst monitor detected a TGF from this lightning, showing that volcanic lightning can also produce TGFs. Any storm with electric fields strong enough to accelerate electrons to high energies is able to produce gamma-ray flashes.

1 Introduction

Since their discovery, TGFs have been associated with lightning and thunderstorms (Fishman et al., 1994). Observations show that TGFs observed from space are produced by intracloud lightning (Dwyer & Smith, 2005; Lu et al., 2010), with the source altitudes of two TGFs measured at ∼12 km (Cummer et al., 2014). Electrons are accelerated to relativistic energies in strong electric fields, either within large-scale fields of thunderstorms (Dwyer, 2008) or within high-field regions at the tips of lightning leaders (Carlson et al., 2010; Celestin & Pasko, 2011). Gamma rays are produced by bremsstrahlung when the relativistic electrons pass near atomic nuclei. Key questions in TGF science are whether

particular types of lightning (more specific than intracloud) or thunderstorms are more likely to produce TGFs. Several investigations have found TGFs to be produced by a variety of thunderstorms ranging in convective strengths, with a preference for strong convection and updrafts. A preference for cold and high cloud tops has also been found (Splitt et al., 2010; Chronis et al., 2015; O. Roberts et al., 2017; Ursi et al., 2019; Tiberia et al., 2021).

2 Observations

Based on the high lightning activity during the December 2021 through January 2022 eruption of the Hunga Tonga–Hunga Ha'apai volcano (Yuen et al., 2022), we searched for TGFs when the Fermi Gamma-ray Burst Monitor (GBM) was within range. As is typical of space-based gamma-ray instruments (Cohen et al., 2010; Gjesteland et al., 2011), GBM can only detect TGFs when the source is within ∼800 km of the sub-satellite point (Connaughton et al., 2013; Briggs et al., 2013) (also Figure A1 of the Appendix). Past ∼300 km, a gamma-ray instrument in low-Earth orbit detects TGF photons scattered out of the main TGF beam by Compton scattering (Østgaard et al., 2008). Past ∼800 km offset, atmospheric attenuation and the amount of scattering required to divert photons to the observing instrument render TGFs undetectable.

Lightning can be detected at long range by their radio emissions. Figure 1 shows the volcanic lightning rate based on VLF radio detections by the World Wide Lightning Network (WWLLN) (Hutchins et al., 2012) for a portion of January 15th and also the times of orbital passes during which GBM was within range. A TGF is detected at 08:52:40 UT using the standard GBM criteria (Briggs et al., 2013; O. J. Roberts et al., 2018). Maps of the WWLLN lightning localizations within ±60 s of the TGF are shown in Figure 2. Also shown are the two closest in time optical detections of lightning by the Geostationary Lightning Mapper (GLM) on GOES-17 (Rudlosky et al., 2019). While GLM missed most of the volcanic lightning due to the opacity of the ash plume, it does not suffer deadtime due to high lightning rates, so that GLM remains highly efficient at detecting thunderstorm lightning. As the only lightning within the TGF-detection range of Fermi GBM originates from the Hunga Tonga–Hunga Ha'apai volcano plume, we conclude that the TGF was produced by volcanic lightning.

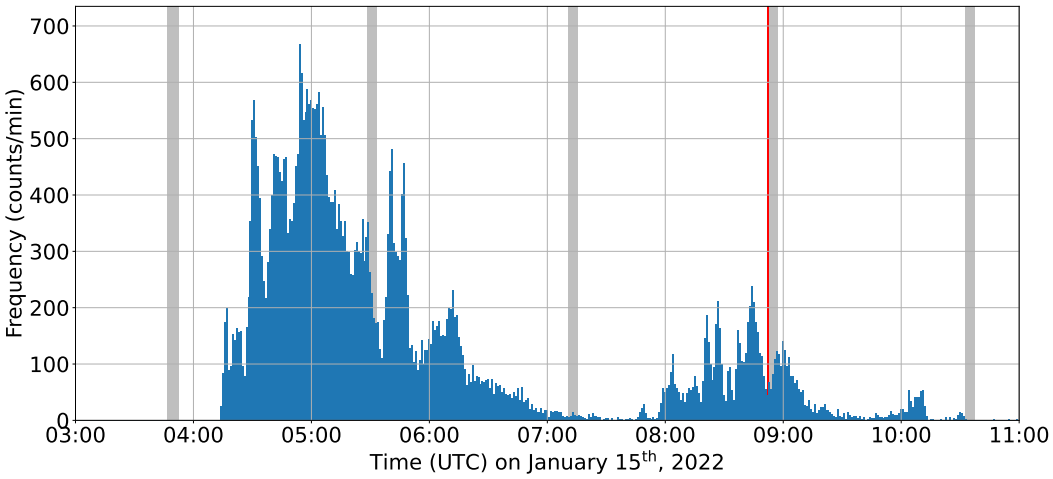

Figure 1. The blue histogram shows the rate of lightning detected by WWLLN within 400 km radius of the Hunga Tonga–Hunga Ha'apai volcano. The grey bars indicate times when Fermi was within 1000 km of the volcano and the red line indicates the time of the TGF detection.

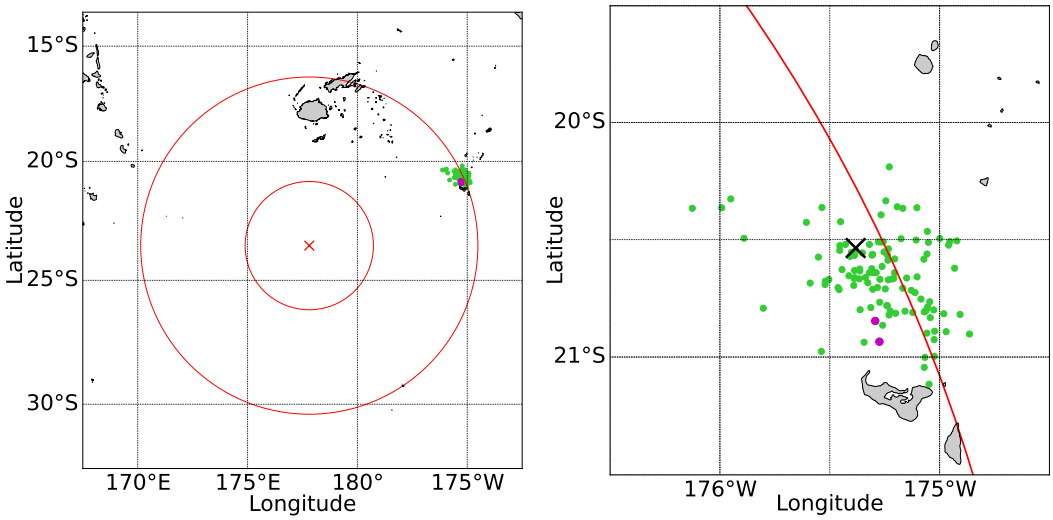

Figure 2. Green points designate lightning radio signals (sferics) detected by WWLLN within ±1 min of the TGF. The magenta points denote the two closest in time optical detections by GLM. Left: A map of lightning activity within the observing range of Fermi GBM. The red cross denotes the sub-satellite point of Fermi at the time of the TGF. The inner red circle has a radius of 300 km around the sub-satellite point, and the outer circle has a radius of 800 km, the approximate limit of TGF detectability for Fermi GBM. Right: Closeup of the volcanic lightning. The black cross denotes the location of Hunga Tonga–Hunga Ha'apai volcano.

Figure 3 shows a time history of gamma-rays detected by the two GBM Bismuth Germanate (BGO) detectors (Meegan et al., 2009). Fermi was oriented to give BGO 1 much better exposure to the volcano than BGO 0. BGO 1 detected more gamma-rays than BGO 0 which is consistent with the TGF originating from the direction of the volcano. The photons are low energy for a TGF; the maximum photon energy is only 970 keV. This spectrum is characteristic of a TGF source at a large offset, with the photon energies decreased due to multiple Compton scatterings. Figure 1 of Mailyan et al. (2016) shows that TGFs observed at low offsets have maximum energies of 10 to 40 MeV, while a TGF at 475 km offset reached only 3 MeV. The spectrum for this TGF is consistent with Figure 1, which shows the closest WWLLN localization at an offset of 719 km from the Fermi sub-satellite point. Only 1.9% of GBM TGFs are detected at larger offsets (see Figure A1).

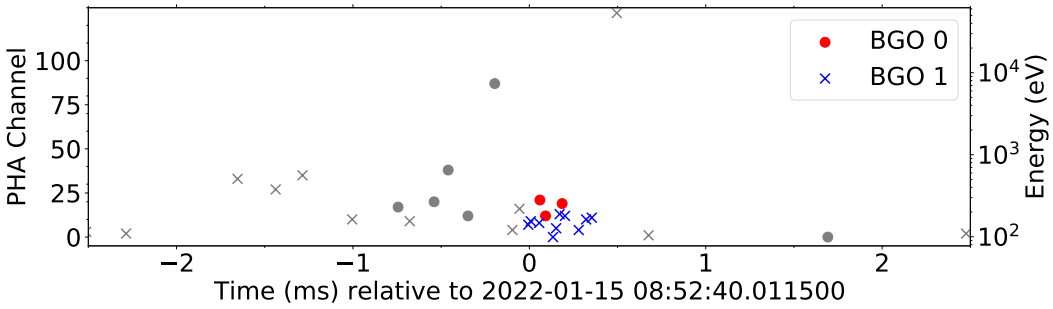

Figure 3. Particles detected by the two GBM Bismuth Germanate (BGO) detectors over 5 ms. An automated analysis selects a 0.4 ms interval for the TGF starting at 08:52:40.011500 UTC ($t = 0$). Photons within this interval belong to the TGF and are shown with colored symbols, red for BGO 0 and blue for BGO 1. The counts outside of this interval are mostly background; perhaps two immediately before $t = 0$ are part of the TGF.

Both WWLLN and ENTLN report the closest sferic in time as 1.28 s after the TGF (the measurements are consistent with being the same sferic). The closest sferics in the GLD360 dataset are 11 ms before and 29 ms after the TGF. The two closest in time optical detections by GLM are 210 s before and 237 s after the TGF. These time differences are corrected 3 ms for the light travel time to Fermi, located at 177.81°E, 23.56°S and 534.4 km altitude at the time of the TGF. The procedure developed for GBM TGFs and WWLLN sferics (O. J. Roberts et al., 2018) is to consider TGFs and sferics within

$\pm$200 μs to be simultaneous and, as such, very likely physically related. WWLLN sferics within $\pm$3.5 ms of a TGF are considered associated with the TGF, perhaps arising from a different lightning step than the simultaneous one. For the $\pm$3.5 ms window, the typical probability of a false association due to unrelated lightning is $\sim$0.1%. When the ambient lightning rate is very high the false association rate can be $\sim$1%. The observed sferics are well outside of the standard association window and so cannot be confidently connected to the TGF, especially considering the extremely high lightning rate from the eruption. With regular thunderstorms, with this procedure associations between GBM TGFs and WWLLN are only found 1/3 of the time (O. J. Roberts et al., 2018). The radio-based lightning networks very likely experienced high deadtimes due to the extremely high lightning rates from the eruption, so it is more likely that the sferic associated with the TGF was missed. The optical flash of the lightning that produced the TGF is very likely obscured to GLM by the ash plume.

3 Analysis

We estimated how many TGFs Fermi GBM should have detected if the volcanic lightning produced TGFs at the same rate as thunderstorm lightning. Briggs et al. (2013) estimated the fraction of lightning flashes that produce TGFs above the detection threshold of GBM. The 2013 GBM TGF sample was compared to the High Resolution Annualized Climatology gridded database of the Lightning Imaging Sensor (LIS). As GBM's TGF detection efficiency decreases with distance from the sub-satellite point, an empirical detection efficiency curve was used to weight the LIS lightning within range of Fermi. The result of this analysis shows that approximately 1 of every 2600 LIS lightning flashes produces a TGF detectable by Fermi GBM.

To go in the reverse direction, i.e., to estimate the expected number of Fermi GBM TGF detections from the observed number of lightning flashes, we need continuous observations of the volcanic lightning from an instrument with a detection efficiency comparable to LIS. Rudlosky et al. (2017) compared the relative detection efficiencies of GLD360 and LIS and found that the detection efficiency of GLD360 improved from 2012 to 2014, and that in 2014, GLD360 generally had relative detection efficiencies greater than 40%, with some areas exceeding 60%. Typically the relative detection efficiency of GLD360 is higher over ocean compared to land. While the regional variations and improving trend make the precise relative detection efficiency of GLD360 to LIS for the Pacific in 2022

uncertain, it is likely high. We therefore use the GLD360 data to estimate how many GBM TGF detections are expected from the volcanic lightning, assuming volcanic lightning produces TGFs at the same rate as thunderstorm lightning. We assume that all sferics localized to within 400 km of Hunga Tonga–Hunga Ha'apai were produced by volcanic lightning. For consistency with the derivation of the TGF/lightning production value of $\frac{1}{2600}$, the detection efficiency curve of Briggs et al. (2013) is used. For the orbital passes of Fermi on 2022 January 14th and 15th, 877 volcanic sferics are found within 300 km of Fermi, and 17444 within 800 km. Weighting by the detection efficiency as a function of offset and the TGF production fraction $\frac{1}{2600}$, a prediction of 1.8 TGFs is found.

There are uncertainties in this estimate: the TGF/lightning efficiency for thunderstorms varies geographically, the TGF/lightning ratio has been calculated for all lightning, while space-observed TGFs are produced by intraclould lightning, and the lightning datasets differ between Briggs et al. (2013) and this calculation. Allowing for these uncertainties, the estimate is still useful to show that the TGF production rate from the volcanic lightning of Hunga Tonga–Hunga Ha'apai is consistent with the average TGF production rate of thunderstorms.

4 Interpretation

There are two possibilities for the accelerated charged particles that produced the observed gamma rays, and thus the orientation of the dipole that accelerated the charged particles. The first is a conventional upward-directed TGF, in which electrons are accelerated upward from a lower negatively charged region to an upper positively charged region. The second is a downward-directed TGF, in which electrons are accelerated downward from an upper negatively charged region to a lower positively charged region. In this case, the GBM observation would be of gamma rays produced by the reverse positron beam. Positron beams have been observed from below an upward-directed TGFs (Bowers et al., 2018) and from space from a downward-directed TGF (Pu et al., 2020). The reverse positron beam is expected to be ∼100 times weaker than the electron beam, reducing its detectability. Partially improving the detectability, the average gamma-ray energy is higher and the beam narrower (Ortberg et al., 2020). The positron-beam TGF detected by Fermi GBM is consistent with these predictions: The TGF was at the detection threshold of GBM, had a high-energy gamma ray (> 10 MeV) and was observed at the low offset of 117 km (Pu et al., 2020). The TGF from the volcanic lightning was

at the very large offset of ∼700 km and had a spectrum consistent with gamma rays Compton scattered from the primary beam. It is implausible that the an already weak positron-beam TGF would be detectable to GBM outside of the beam, via Compton scattered photons. We therefore conclude that the TGF is a typical upward-directed TGF, indicating that the electrons were accelerated by a dipole configuration of positive above negative charge, which is different from some charge structures observed in weaker eruptions (Behnke et al., 2014).

To our knowledge, this is the first TGF detected from volcanic lightning. Charge separation to create electric fields in thunderstorms is thought to occur by convection and the collisions of soft hail (graupel) and ice crystals (Saunders, 2008). Volcanic plumes can electrify through ash charging mechanisms, fracturing and collisions (friction), and also from grauple-ice collisions as in regular thunderstorms (Behnke et al., 2014; Cimarelli & Genareau, 2022). As a submarine volcano, the plume of Hunga Tonga–Hunga Ha'apai likely had a large amount of entrained water (Yuen et al., 2022), so that water-based mechanisms likely dominated the electrification process. High lightning rates are observed in volcanic plumes when the plumes reach altitudes that are cold enough for ice formation; also higher plumes correlate with stronger updrafts which increase electrification in regular thunderstorms (Behnke et al., 2012; Van Eaton et al., 2022). Based on the number of lightning flashes detected by GLD360 when Fermi GBM was within range, and assuming that the TGF production efficiency from the volcanic lightning is the same as thunderstorm lightning, we estimate that GBM should have detected ∼2 TGFs during the very high lightning rates of the 2022 January 14–15 eruption. The observation of a single TGF from the Hunga Tonga-Hunga Ha'apai erruption is fully consistent with this estimate, suggesting that the volcanic plume produced TGFs in a manner similar to that of ordinary thunderstorms. The observation of a TGF from volcanic lightning extends the observations that a variety of thunderstorms can produce TGFs, showing that as long as a storm is able to produce electrification sufficient to accelerate electrons to relativistic energies, it can produce TGFs.

Appendix A TGF detection efficiency with distance from Fermi

Figure 8 of Briggs et al. (2013) shows the distribution of GBM TGF distances from the Fermi sub-satellite point, using the sample of 141 TGFs with WWLLN associations available at the time. TGFs with WWLLN associations are used because WWLLN pro-

vides locations of ∼20 km accuracy, while Fermi GBM is unable to localize TGFs. The online Fermi GBM TGF catalog, `https://fermi.gsfc.nasa.gov/ssc/data/access/gbm/tgf/` (O. J. Roberts et al., 2018), provides a sample of 1544 GBM TGFs with WWLLN associations, so we repeat that analysis to determine the TGF offset distribution with better statistics: Figure A1a.

The paucity of TGFs at small offsets in Figure A1a is because there is very little Earth area being observed at these radii. Figure A1b shows the curve normalized by the observed area of the Earth (Gjesteland et al., 2011; O. J. Roberts et al., 2018), which better displays TGF intrinsic properties. Up to ∼250 km, TGFs are observed within their primary beam and the detection rate is high. Past this offset, gamma-rays reach GBM by being Compton scattered out of the primary beam. The TGFs appear fainter and the detection rate falls as the offset becomes larger.

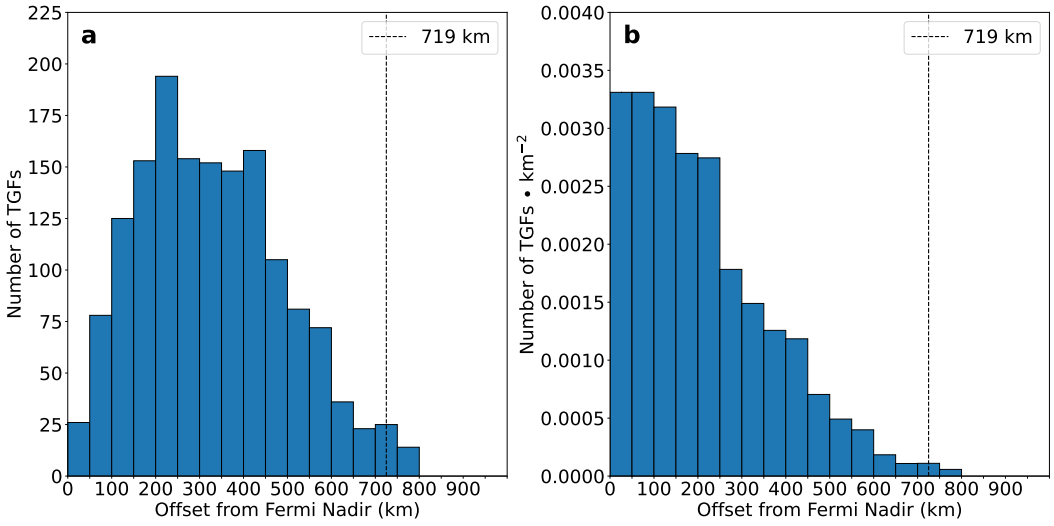

Figure A1. a: The number of TGFs with WWLLN associations detected by Fermi GBM versus distance between the Fermi sub-satellite point and the WWLLN determined location. b: The same data, corrected to be a rate per area of the Earth. The vertical dashed line indicates the distance between the Fermi sub-satellite point and the nearest WWLLN sferic on the map shown in Fig. 2.

Appendix B Open Research

Fermi-GBM data (Fermi GBM Team, 2022) are available at `https://fermi.gsfc.nasa.gov/ssc/data/access/gbm/`. These data are available un-

der NASA's open data policy. GLM data (GLM Team, 2022) are available as GOES-R Series GLM L2+ Data Product (GRGLMPROD) from `https://www.avl.class.noaa.gov/saa/products/search?datatype_family=GRGLMPROD`. These data are available under NOAA's open data policy. The WWLLN data used in this paper are posted on a Zenodo repository (Briggs et al., 2022), available under Creative Commons Attribution 4.0 International License. The GLD360 data used in this paper are available for research use from Vaisala (Vaisala, 2022) upon request and signing a data usage agreement, and are not accessible to the public or research community. Researchers may contact Vaisala at `https://www.vaisala.com/en/lp/contact-us-lightning-solutions` to arrange research use of GLD360 data (Vaisala, 2022). The single ENTLN sferic cited in this paper is identical to WWLLN sferic #46 in the WWLLN list available in the Zenodo dataset (see above). The ENTLN data used in this are available for research use from Earth Networks (Earth Networks, 2022) upon request and signing a data usage agreement, and are not accessible to the public or research community. Researchers may contact ENTLN at `customercare@earthnetworks.com` to arrange research use of Earth Networks Total Lightning Network (ENTLN) data.

Acknowledgments

The authors express their sympathies to those harmed by the eruption of Hunga Tonga–Hunga Ha'apai. We thank D. Smith for the suggestion to search for a TGF from the eruption and S. A. Behnke for helpful comments. The Fermi-GBM Collaboration acknowledges the support of NASA in the United States through NNM11AA01A and DRL in Germany. The authors wish to thank the World Wide Lightning Location Network (`wwlln.net`), a collaboration among over 50 universities and institutions, for providing lightning location data used in this paper. We thank Vaisala for the use of the GLD360 lightning data. We also thank Earth Networks for providing the ENTLN lightning data that was used in this study.

References

Behnke, S. A., Thomas, R. J., Edens, H. E., Krehbiel, P. R., & Rison, W. (2014). The 2010 eruption of eyjafjallajkull: Lightning and plume charge structure. *Journal of Geophysical Research: Atmospheres*, *119*(2), 833-859. Retrieved

from https://agupubs.onlinelibrary.wiley.com/doi/abs/10.1002/2013JD020781 doi: https://doi.org/10.1002/2013JD020781

Behnke, S. A., Thomas, R. J., Krehbiel, P. R., & McNutt, S. R. (2012). Spectacular lightning revealed in 2009 mount redoubt eruption. *Eos, Transactions American Geophysical Union*, *93*(20), 193-194. Retrieved from https://agupubs.onlinelibrary.wiley.com/doi/abs/10.1029/2012EO200001 doi: https://doi.org/10.1029/2012EO200001

Bowers, G. S., Smith, D. M., Kelley, N. A., Martinez-McKinney, G. F., Cummer, S. A., Dwyer, J. R., ... Rassoul, H. K. (2018). A terrestrial gamma-ray flash inside the eyewall of hurricane patricia. *Journal of Geophysical Research: Atmospheres*, *123*(10), 4977-4987. Retrieved from https://agupubs.onlinelibrary.wiley.com/doi/abs/10.1029/2017JD027771 doi: https://doi.org/10.1029/2017JD027771

Briggs, M. S., Lesage, S., Schultz, C., Mailyan, B., & Holzworth, R. H. (2022). *Wwlln datasets for "a terrestrial gamma-ray flash from the 2022 hunga tonga–hunga ha'apai volcanic eruption"* [dataset]. Retrieved from https://doi.org/10.5281/zenodo.6782049 doi: https://doi.org/10.5281/zenodo.6782049

Briggs, M. S., Xiong, S., Connaughton, V., Tierney, D., Fitzpatrick, G., Foley, S., ... Hutchins, M. L. (2013). Terrestrial gamma-ray flashes in the Fermi era: Improved observations and analysis methods. *J. Geophys. Res. Space Physics*, *118*, 3805–3830. Retrieved from https://agupubs.onlinelibrary.wiley.com/doi/abs/10.1002/jgra.50205 doi: 10.1002/jgra.50205

Carlson, B. E., Lehtinen, N. G., & Inan, U. S. (2010). Terrestrial gamma ray flash production by active lightning leader channels. *J. Geophys. Res.*, *115*, A10324. Retrieved from https://agupubs.onlinelibrary.wiley.com/doi/abs/10.1029/2010JA015647 doi: 10.1029/2010JA015647

Celestin, S., & Pasko, V. P. (2011). Energy and fluxes of thermal runaway electrons produced by exponential growth of streamers during the stepping of lightning leaders and in transient luminous events. *J. Geophys. Res.*, *116*, A03315. Retrieved from https://agupubs.onlinelibrary.wiley.com/doi/abs/10.1029/2010JA016260 doi: 10.1029/2010JA016260

Chronis, T., Briggs, M. S., Priftis, G., Connaughton, V., Brundell, J., Holzworth, R.,

... Stanbro, M. (2015). Characteristics of thunderstorms that produce terrestrial gamma-ray flashes. *Bull. Amer. Meteor. Soc.*. Retrieved from https://journals.ametsoc.org/view/journals/bams/97/4/bams-d-14-00239.1.xml doi: 10.1175/BAMS-D-14-00239.1

Cimarelli, C., & Genareau, K. (2022). A review of volcanic electrification of the atmosphere and volcanic lightning. *Journal of Volcanology and Geothermal Research*, *422*, 107449. Retrieved from https://www.sciencedirect.com/science/article/pii/S037702732100278X doi: https://doi.org/10.1016/j.jvolgeores.2021.107449

Cohen, M. B., Inan, U. S., Said, R. K., & Gjestland, T. (2010). Geolocation of terrestrial gamma-ray flash source lightning. *Geophys. Res. Lett.*, *37*. Retrieved from https://agupubs.onlinelibrary.wiley.com/doi/abs/10.1029/2009GL041753 doi: 10.1029/2009GL041753

Connaughton, V., Briggs, M. S., Xiong, S., Dwyer, J. R., Hutchins, M. L., Grove, J. E., ... Wilson-Hodge, C. (2013). Radio signals from electron beams in terrestrial gamma-ray flashes. *J. Geophys. Res. Space Physics*, *118*, 2313–2320. Retrieved from https://agupubs.onlinelibrary.wiley.com/doi/abs/10.1029/2012JA018288 doi: 10.1029/2012JA018288

Cummer, S. A., Briggs, M. S., Dwyer, J. R., Xiong, S., Connaughton, V., Fishman, G. J., ... Solanki, R. (2014). The source altitude, electric current, and intrinsic brightness of terrestrial gamma ray flashes. *Geophys. Res. Lett.*. Retrieved from https://agupubs.onlinelibrary.wiley.com/doi/abs/10.1002/2014GL062196 doi: 10.1002/2014GL062196

Dwyer, J. R. (2008). Source mechanisms of terrestrial gamma-ray flashes. *J. Geophys. Res.*, *113*, D10103. Retrieved from https://agupubs.onlinelibrary.wiley.com/doi/abs/10.1029/2007JD009248 doi: 10.1029/2007JD009248

Dwyer, J. R., & Smith, D. M. (2005). A comparison between monte carlo simulations of runaway breakdown and terrestrial gamma-ray flash observations. *Geophys. Res. Lett.*, *32*, L22804. Retrieved from https://agupubs.onlinelibrary.wiley.com/doi/abs/10.1029/2005GL023848 doi: 10.1029/2005GL023848

Earth Networks. (2022). *Earth networks total lightning network (ENTLN) data* [dataset]. Earth Networks. Retrieved from https://www.earthnetworks.com

Fermi GBM Team. (2022). *Fermi gamma-ray burst monitor (GBM) data* [dataset]. Retrieved from https://fermi.gsfc.nasa.gov/ssc/data/access/gbm/

Fishman, G. J., Bhat, P. N., Mallozzi, R., Horack, J. M., Koshut, T., Kouveliotou, C., ... Christian, H. J. (1994). Discovery of intense gamma-ray flashes of atmospheric origin. *Science*, *264*, 1313–1316. Retrieved from https://www.science.org/doi/abs/10.1126/science.264.5163.1313 doi: 10.1126/science.264.5163.1313

Gjesteland, T., Østgaard, N., Collier, A. B., Carlson, B. E., Cohen, M. B., & Lehtinen, N. G. (2011). Confining the angular distribution of terrestrial gamma ray flash emission. *J. Geophys. Res.*, *116*, A11313. Retrieved from https://agupubs.onlinelibrary.wiley.com/doi/abs/10.1029/2011JA016716 doi: 10.1029/2011JA016716

GLM Team. (2022). *Geostationary lightning mapper (GLM) data* [dataset]. NOAA. Retrieved from https://www.avl.class.noaa.gov/saa/products/search?datatype_family=GRGLMPROD

Hutchins, M. L., Holzworth, R. H., Brundell, J. B., & Rodger, C. J. (2012). Relative detection efficiency of the world wide lightning location network. *Radio Sci*, *47*, RS6005. Retrieved from https://agupubs.onlinelibrary.wiley.com/doi/abs/10.1029/2012RS005049 doi: 10.1029/2012RS005049

Lu, G., Blakeslee, R. J., Li, J., Smith, D. M., Shao, X.-M., McCaul, E. W., ... Cummer, S. A. (2010). Lightning mapping observation of a terrestrial gamma-ray flash. *Geophys. Res. Lett.*, *37*, L11806. Retrieved from https://agupubs.onlinelibrary.wiley.com/doi/abs/10.1029/2010GL043494 doi: 10.1029/2010GL043494

Mailyan, B. G., Briggs, M. S., Cramer, E. S., Fitzpatrick, G., Roberts, O. J., Stanbro, M., ... Dwyer, J. R. (2016). The spectroscopy of individual terrestrial gamma-ray flashes: Constraining the source properties. *Journal of Geophysical Research: Space Physics*, *121*(11), 346–363. Retrieved from https://agupubs.onlinelibrary.wiley.com/doi/abs/10.1002/2016JA022702 doi: 10.1002/2016JA022702

Meegan, C. A., Lichti, G., Bhat, P. N., Bissaldi, E., Briggs, M. S., Connaughton, V., ... Wilson-Hodge, C. (2009). The Fermi gamma-ray burst monitor. *ApJ*, *702*, 791–804. Retrieved from https://doi.org/10.1088/0004-637x/702/1/791

doi: 10.1088/0004-637X/702/1/791

Ortberg, J., Smith, D. M., Li, J., Dwyer, J., & Bowers, G. (2020). Detecting an upward terrestrial gamma ray flash from its reverse positron beam. *Journal of Geophysical Research: Atmospheres*, *125*(6), e2019JD030942. Retrieved from https://agupubs.onlinelibrary.wiley.com/doi/abs/10.1029/2019JD030942 doi: https://doi.org/10.1029/2019JD030942

Østgaard, N., Gjesteland, T., Stadsnes, J., Connell, P. H., & Carlson, B. (2008). Production altitude and time delays of the terrestial gamma flashes: Revisiting the burst and transient source experiment spectra. *Journal of Geophys. Res.*, *113*, A02307. Retrieved from https://agupubs.onlinelibrary.wiley.com/doi/abs/10.1029/2007JA012618 doi: 10.1029/2007JA012618

Pu, Y., Cummer, S. A., Huang, A., Briggs, M., Mailyan, B., & Lesage, S. (2020). A satellite-detected terrestrial gamma ray flash produced by a cloud-to-ground lightning leader. *Geophysical Research Letters*, *47*(15), e2020GL089427. Retrieved from https://agupubs.onlinelibrary.wiley.com/doi/abs/10.1029/2020GL089427 doi: https://doi.org/10.1029/2020GL089427

Roberts, O., Chronis, T., Fitzpatrick, G., Bedka, K., McBreen, S., Briggs, M., ... Stanbro, M. (2017). Terrestrial gamma-ray flashes due to particle acceleration in tropical storm systems. *JGR*. Retrieved from https://agupubs.onlinelibrary.wiley.com/doi/abs/10.1002/2016JD025799 doi: 10.1002/2016JD025799

Roberts, O. J., Fitzpatrick, G., Stanbro, M., McBreen, S., Briggs, M. S., Holzworth, R. H., ... Mailyan, B. G. (2018). The first fermi-gbm terrestrial gamma ray flash catalog. *Journal of Geophysical Research: Space Physics*, *123*(5), 4381-4401. Retrieved from https://agupubs.onlinelibrary.wiley.com/doi/abs/10.1029/2017JA024837 doi: 10.1029/2017JA024837

Rudlosky, S. D., Goodman, S. J., Virts, K. S., & Bruning, E. C. (2019). Initial geostationary lightning mapper observations. *Geophysical Research Letters*, *46*(2), 1097-1104. Retrieved from https://agupubs.onlinelibrary.wiley.com/doi/abs/10.1029/2018GL081052 doi: https://doi.org/10.1029/2018GL081052

Rudlosky, S. D., Peterson, M. J., & Kahn, D. T. (2017). GLD360 performance relative to TRMM LIS. *Journal of Atmospheric and Oceanic Technology*,

34(6), 1307 - 1322. Retrieved from https://journals.ametsoc.org/view/journals/atot/34/6/jtech-d-16-0243.1.xml doi: 10.1175/JTECH-D-16-0243.1

Saunders, C. (2008). Charge separation mechanisms in clouds. *Space Science Reviews*, *137*, 335–353. Retrieved from https://doi.org/10.1007/s11214-008-9345-0 doi: 10.1007/s11214-008-9345-0

Splitt, M. E., Lazarus, S. M., Barnes, D., Dwyer, J. R., Rassoul, H. K., Smith, D. M., ... Grefenstette, B. (2010). Thunderstorm characteristics associated with RHESSI identified terrestrial gamma ray flashes. *J. Geophys. Res.*, *115*, A00E38. Retrieved from https://agupubs.onlinelibrary.wiley.com/doi/abs/10.1029/2009JA014622 doi: 10.1029/2009JA014622

Tiberia, A., Mascitelli, A., D'Adderio, L. P., Federico, S., Marisaldi, M., Porcù, F., ... Dietrich, S. (2021). Time evolution of storms producing terrestrial gamma-ray flashes using era5 reanalysis data, gps, lightning and geostationary satellite observations. *Remote Sensing*, *13*(4). Retrieved from https://www.mdpi.com/2072-4292/13/4/784 doi: 10.3390/rs13040784

Ursi, A., Marisaldi, M., Dietrich, S., Tavani, M., Tiberia, A., & Porcù, F. (2019). Analysis of thunderstorms producing terrestrial gamma ray flashes with the meteosat second generation. *Journal of Geophysical Research: Atmospheres*, *124*(23), 12667-12682. Retrieved from https://agupubs.onlinelibrary.wiley.com/doi/abs/10.1029/2018JD030149 doi: https://doi.org/10.1029/2018JD030149

Vaisala. (2022). *Global lightning detection network GLD360 data* [dataset]. Vaisala. Retrieved from https://www.vaisala.com/en/products/systems/lightning/gld360

Van Eaton, A. R., Smith, C. M., Pavolonis, M., & Said, R. (2022, 01). Eruption dynamics leading to a volcanic thunderstorm—The January 2020 eruption of Taal volcano, Philippines. *Geology*, *50*(4), 491-495. Retrieved from https://doi.org/10.1130/G49490.1 doi: 10.1130/G49490.1

Yuen, D. A., Scruggs, M. A., Spera, F. J., Zheng, Y., Hu, H., McNutt, S. R., ... Tanioka, Y. (2022). Under the surface: Pressure-induced planetary-scale waves, volcanic lightning, and gaseous clouds caused by the submarine eruption of hunga tonga-hunga ha'apai volcano. *Earthquake Research Advances*,

100134. Retrieved from https://www.sciencedirect.com/science/article/pii/S2772467022000227 doi: https://doi.org/10.1016/j.eqrea.2022.100134